

Searching for dark matter with a 1000 km baseline interferometer

Daniel Gavilan-Martin,^{1,2,*} Grzegorz Łukasiewicz,^{3,4,*} Mikhail Padniuk,³ Emmanuel Klinger,⁵ Magdalena Smolis,³ Nataniel L. Figueroa,^{1,2} Derek F. Jackson Kimball,⁶ Alexander O. Sushkov,^{7,8,9,10} Szymon Pustelny,³ Dmitry Budker,^{1,2,11} and Arne Wickenbrock^{1,2}

¹*Johannes Gutenberg-Universität Mainz, 55128 Mainz, Germany*

²*Helmholtz-Institut Mainz, GSI Helmholtzzentrum für Schwerionenforschung, 55128 Mainz, Germany*

³*Marian Smoluchowski Institute of Physics, Jagiellonian University in Kraków, Łojasiewicza 11, 30-348, Kraków, Poland*

⁴*Doctoral School of Exact and Natural Sciences,*

Jagiellonian University in Kraków, Łojasiewicza 11, 30-348, Kraków, Poland

⁵*Institut FEMTO-ST – UMR 6174 CNRS, SupMicroTech-ENSMM,*

Université de Franche-Comté, 25030 Besançon, France

⁶*Department of Physics, California State University – East Bay, Hayward, CA 94542, USA*

⁷*Department of Physics, Boston University, Boston, MA 02215, USA*

⁸*Department of Electrical and Computer Engineering, Boston University, Boston, MA 02215, USA*

⁹*Photonics Center, Boston University, Boston, MA 02215, USA*

¹⁰*Department of Physics & Astronomy, The Johns Hopkins University, Baltimore, MD 21218, USA*

¹¹*Department of Physics, University of California, Berkeley, CA 94720, USA*

Axion-like particles (ALPs) arise from well-motivated extensions to the Standard Model and could account for dark matter. ALP dark matter would manifest as a nearly monochromatic field oscillating at an (as of yet) unknown frequency. The frequency depends on the ALP mass, which could plausibly range from 10^{-22} eV/ c^2 to 10 eV/ c^2 . We report on a direct search for ALP dark matter through the ALP-nucleon interaction by interfering the signals of two atomic K-Rb-³He comagnetometers, with one situated in Mainz, Germany, and the other in Kraków, Poland. We use the ALP dark matter’s spatiotemporal coherence properties assuming the standard halo model of dark matter in the Milky Way to improve the sensitivity and exclude spurious candidates. The search extends over nine orders of magnitude in ALP mass. In this range, no significant evidence of an ALP signal is found. We thus place new upper limits on the ALP-neutron and ALP-proton couplings of $g_{aNN} < 10^{-5}$ GeV⁻¹ and $g_{aPP} < 5 \times 10^{-4}$ GeV⁻¹ at a mass of 10^{-22} eV/ c^2 and extending to a mass of 10^{-15} eV/ c^2 where the upper limits reach below $g_{aNN} < 10^{-9}$ GeV⁻¹ and $g_{aPP} < 10^{-7}$ GeV⁻¹, respectively. For both neutron and proton couplings, this work is an improvement of up to four orders of magnitude compared to previous laboratory constraints.

I. INTRODUCTION

Abundant astrophysical and cosmological observations at different scales [1–3] suggest that about 85% of the matter in the Universe does not noticeably interact with electromagnetic fields and is thus known as “dark” matter (DM). Its composition is unknown, which makes it a provocative indication of physics beyond the Standard Model (SM) and drives the search for hypothetical DM particles.

Ultralight ($\lesssim 10$ eV/ c^2) pseudoscalars known as axion-like particles (ALPs) are particularly well-motivated DM candidates [4]. ALPs could account for the correct abundance of relic DM (via, for example, a misalignment mechanism [5]) and a subset of them could resolve the strong-CP problem [6]. Additionally, ALPs can interact with SM-particles through couplings to photons, gluons, and fermions [7], offering direct ways of probing their existence [8–10].

Here, we present the results of an interferometric [11] ALP search over nine orders of magnitude in mass range. The interferometer is composed of two K-Rb-³He atomic

comagnetometers, one located at the Jagiellonian University in Kraków, Poland and the other, separated by 860 km, at the Johannes Gutenberg University in Mainz, Germany (see Fig. 1(a)). The interference occurs in the phase sensitive combination of the amplitude data, similar to interference phenomena in radio telescope networks such as the event horizon telescope [12]. The main difference being that our interferometer is sensitive to ALP DM waves rather than electromagnetic waves.

Both comagnetometers are optimized to operate in the self-compensated regime [13–15]. To first order, the devices are insensitive to low-frequency magnetic field variations, but retain sensitivity to non-magnetic spin interactions [16, 17]. This makes them excellent tools for probing the interaction of the galactic ALP DM field $a(\mathbf{r}, t)$ with neutron spins $\boldsymbol{\sigma}_N$ or proton spins $\boldsymbol{\sigma}_P$. The ALP-nucleon is a gradient interaction and described by the Hamiltonians

$$\begin{aligned}\mathcal{H}_N &= g_{aNN} \nabla a \cdot \boldsymbol{\sigma}_N, \\ \mathcal{H}_P &= g_{aPP} \nabla a \cdot \boldsymbol{\sigma}_P,\end{aligned}\tag{1}$$

where g_{aNN} and g_{aPP} are unknown coupling constants to neutrons and protons associated with the interaction.

Self-compensating comagnetometers have already established the most stringent limits in certain mass ranges, even surpassing astrophysical constraints [18–20].

* Both authors contributed equally.

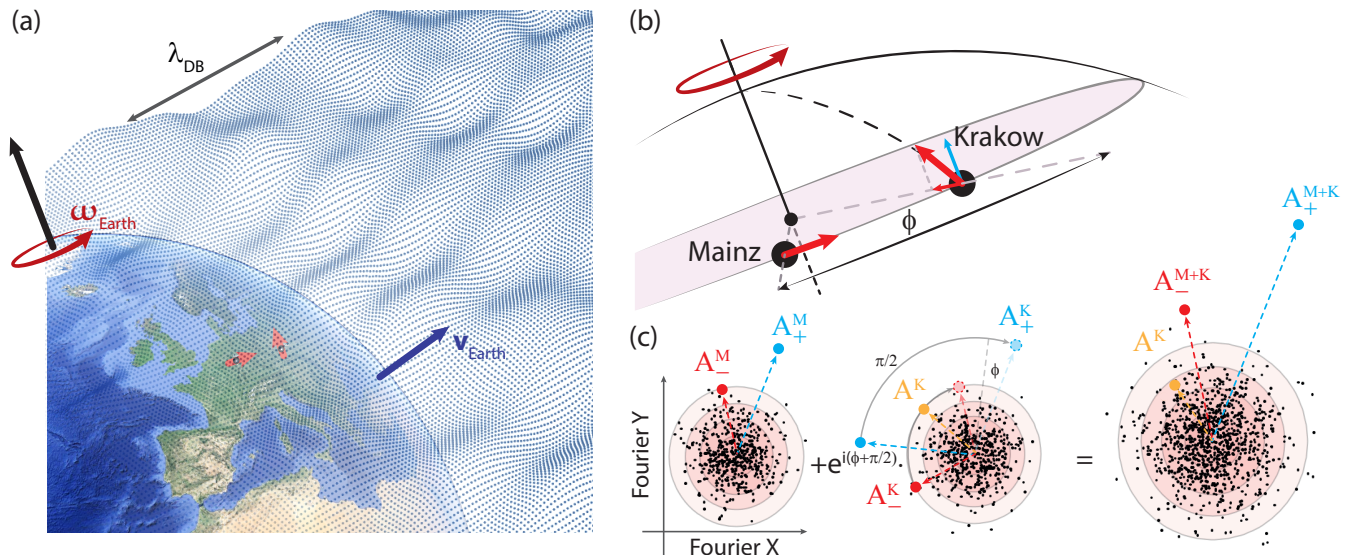


FIG. 1. (a) Interferometer schematic. The two comagnetometers comprising the interferometer are indicated in their respective host cities Mainz and Kraków. The red arrows point in the direction of their respective sensitivity axes. Earth is rotating at the sidereal frequency ω_e and moving at velocity v_e with respect to the galactic rest frame through the ALP DM field, characterized by its de Broglie wavelength λ_{DB} . Note, that the smallest de Broglie wavelength in the presented search is more than a thousand times larger than the radius of the Earth. (b) Orientation of the sensitive axes of the comagnetometer stations with respect to the rotation axis of the Earth. The sensitive axes of the comagnetometers can be decomposed into components along the rotation axis and perpendicular to it. The former results in an ALP signal component at the Compton frequency of the ALP constituent particle (carrier) while the latter results in (generally asymmetric) sidebands separated from the carrier by the sidereal frequency. (c) Signal interferometry in the data analysis. ALP constituents in this search would have the same properties in Mainz and Kraków and would appear as signals at the carrier and sideband frequencies. Both stations would detect sideband signals while the carrier signal would only appear in the Kraków data. To coherently add ALP signals from Mainz and Kraków, the phase differences due to the different sensitive axis orientation ($\pi/2$) as well as due to the different locations (ϕ) need to be taken into account. In this way, the signal amplitudes add linearly while the noise adds in quadrature, improving the signal-to-noise ratio by over $\sqrt{2}$. The signals at the three different frequencies, Kraków carrier with amplitude A^K and the combined lower (A_{-}^{K+M}) and upper (A_{+}^{K+M}) sidebands are then combined in quadrature to construct the signal estimator used to search for evidence of ALP DM.

In this work, we search in experimentally-unconstrained ALP parameter space in the ultralight mass range below 10^{-13} eV/ c^2 .

If the estimated local DM density (≈ 0.4 GeV/ cm^3) is mostly due to an ALP of mass m_a , the occupation number of the ALP field would be large and it can be approximated as a classical field oscillating near the ALP Compton frequency [21]. In this model, the characteristics of the oscillating ALP field, such as its amplitude and the direction of the field gradient, fluctuate in time [22–26]. The characteristic time scale of the fluctuations is given by the ALP DM coherence time, which is around 10^6 oscillations of the field (for example, about 15 years for $m_a = 10^{-17}$ eV/ c^2).

Here, we focus primarily on the regime where the coherence time of the collective oscillation is larger than the measurement time. In this regime, the ALP field can be treated as having a constant amplitude and direction. In the considered mass range, the ALP field signature at the two locations is highly correlated. For reference, an ALP particle of mass 10^{-17} eV/ c^2 , assuming a velocity equal to that of Earth in the galactic rest frame ($10^{-3} c$),

has a de Broglie wavelength of $\sim 10^3$ astronomical units. By properly combining the signals from both stations, the ALP signals will be added constructively, while the effects of local noise fluctuations sum incoherently and are suppressed. An additional analysis was done to extend the search to ALP masses below $\sim 5 \times 10^{-20}$ eV/ c^2 ; this analysis consisted of looking for spectral signatures that would appear due to the rotation of Earth. The properties of the field gradient in this ultralow frequency regime are discussed and the signal properties are explicitly reviewed below.

The paper is structured as follows. In Sec. II we review the ALP DM signal model and show explicitly the expected trace in the frequency domain for a daily modulated sensor and discuss the sensitivity improvement of interfering signals of multiple sensors. In section III we show the analysis framework and how data is combined to maximize signal-to-noise ratio. No ALP candidates are found, so we set limits in Sec. IV. The experimental setup and some technical details of the search are presented in Sec. V.

II. SIGNAL MODEL

Here we briefly describe the expected signal model in the two comagnetometers of the interferometer. We utilize the framework described in Refs. [18, 24, 25]. Due to its high occupation number, the ALP field can be approximated as a sum of N independent oscillators. We write the components of the ALP field gradient at position \mathbf{r} and time t in a Cartesian frame of reference $i = x, y, z$ where the Solar System is at rest:

$$\begin{aligned}\nabla_i a(\mathbf{r}, t) &= \frac{\hbar\sqrt{2\rho_{\text{DM}}}}{m_a c\sqrt{N}} \sum_{n=1}^N \nabla_i \sin(\omega_n t - \mathbf{k}_n \cdot \mathbf{r} + \phi_n) \\ &= \frac{\sqrt{2\rho_{\text{DM}}}}{c\sqrt{N}} \sum_n (\mathbf{v}_n)_i \cos(\omega_n t - \mathbf{k}_n \cdot \mathbf{r} + \phi_n),\end{aligned}\quad (2)$$

where the negative sign in the second line is absorbed by the random phase ϕ_n , c is the speed of light, m_a is the ALP mass, $\rho_{\text{DM}} \approx 0.4 \text{ GeV}/\text{cm}^3$ [9] is the local density of dark matter, $\mathbf{k}_n = m_a \mathbf{v}_n / \hbar$ is the wave vector, ω_n is the angular frequency of each oscillating mode n and $(\mathbf{v}_n)_i$ the i -th component of \mathbf{v}_n . Assuming that ALPs are virialized in the Milky Way, the velocities \mathbf{v}_n will follow a 3D normal distribution centered at zero in the galactic frame. On Earth, the observed velocity distribution will be offset by Earth's velocity in the galactic frame $(\mathbf{v}_e)_i$. We neglect effects due to the movement of Earth within the Solar System since it is negligible compared to the velocity of the Solar System in the galaxy [25]. The velocity components $(\mathbf{v}_n)_i$ are distributed according to

$$f(v_i) = \frac{1}{v_0\sqrt{\pi}} \exp\left\{-\left[\frac{v_i - (\mathbf{v}_e)_i}{v_0}\right]^2\right\}, \quad (3)$$

where $v_0 \approx 220 \text{ km/s}$ is the virial velocity in the galaxy, which determines the variance of the velocity distribution as $v_0^2/2$.

Each mode of the ALP field experiences a kinetic energy correction leading to a small frequency shift $\omega_n \approx \omega_a(1 + \mathbf{v}_n^2/2c^2)$. Most of the ALP spectrum is concentrated within a spectral width given by [25]

$$\Delta\omega \approx \omega_a \frac{v_0^2}{c^2} \approx \omega_a \times 10^{-6}. \quad (4)$$

The collective mode can be described by a nearly monochromatic oscillation with independent amplitude and phase for each orthogonal spatial direction. The amplitudes and phases are random and evolve smoothly on time scales set by the coherence time $\tau \approx 2\pi/\Delta\omega$. The underlying probability distributions of the amplitudes and phases can be derived from Eqs. (2) and (3) [25]. This results in six independent parameters: three amplitudes (α_x , α_y , and α_z) following Rayleigh distributions and three phases (ϕ_x , ϕ_y , and ϕ_z) following uniform distributions over $[0, 2\pi)$ [24]. Because the ALP de Broglie wavelength in the analyzed mass range is much larger than the sensor separation, $\lambda = 2\pi/k_n \gg d = 860 \text{ km}$, we neglect the spatial dependence, i.e. $\mathbf{k}_n \cdot \mathbf{r} \approx 0$, in Eq. (2) for both sensors. The ALP gradient can then be written as

$$\begin{aligned}\nabla a(t) &= \frac{\sqrt{2\rho_{\text{DM}}}}{c\sqrt{N}} \sum_n \mathbf{v}_n \cos(\omega_a t + \phi_n) \\ &= \hat{\mathbf{x}}\alpha_x \cos(\omega_a t + \phi_x) + \hat{\mathbf{y}}\alpha_y \cos(\omega_a t + \phi_y) \\ &\quad + \hat{\mathbf{z}}\alpha_z \cos(\omega_a t + \phi_z),\end{aligned}\quad (5)$$

where the summation of the first line manifests in the second line as the amplitudes α_i . The probability distributions of the amplitudes α_i are given by

$$\alpha_i \sim \frac{\sqrt{2\rho_{\text{DM}}}}{c} \sqrt{\frac{v_0^2/2 + (\mathbf{v}_e)_i^2}{2}} \alpha. \quad (6)$$

where α is a Rayleigh distributed random number with scale parameter equal to 1.

The sensitive axis $\hat{\mathbf{m}}$ of a single sensor located at the Earth's surface rotates with the sidereal frequency of Earth, ω_e . The coordinate system is chosen such that the $\hat{\mathbf{z}}$ component is parallel to the Earth rotation axis. It can be assumed constant in the galactic rest frame over the timespan of the experiment. This results in a fixed m_z component and daily modulated m_x and m_y components:

$$\begin{aligned}\hat{\mathbf{m}}(t) &= \hat{\mathbf{x}} \sin \theta \sin(\omega_e t + \phi_e) \\ &\quad + \hat{\mathbf{y}} \sin \theta \cos(\omega_e t + \phi_e) \\ &\quad + \hat{\mathbf{z}} \cos \theta,\end{aligned}\quad (7)$$

where $\theta = \angle(\hat{\mathbf{z}}, \hat{\mathbf{m}})$ is the polar angle. The experimental signal is proportional to the projection of the gradient of the ALP field on the sensitive axis of the sensor,

$$\begin{aligned}\nabla a(t) \cdot \hat{\mathbf{m}}(t) &= \frac{\alpha_x \sin \theta}{2} \left\{ \sin [(\omega_a + \omega_e)t + \phi_x + \phi_e] - \sin [(\omega_a - \omega_e)t + \phi_x - \phi_e] \right\} \\ &\quad + \frac{\alpha_y \sin \theta}{2} \left\{ \cos [(\omega_a + \omega_e)t + \phi_y + \phi_e] + \cos [(\omega_a - \omega_e)t + \phi_y - \phi_e] \right\} \\ &\quad + \alpha_z \cos \theta \cos(\omega_a t + \phi_z).\end{aligned}\quad (8)$$

The pseudomagnetic field in the experiment is given by

$B_a = \frac{g_{\text{eff}}}{\mu_n} \nabla a \cdot \hat{\mathbf{m}}$, with μ_n the gyromagnetic ratio of the

nucleus of ${}^3\text{He}$, and $g_{\text{eff}} = g_{aNN}\xi_N$ the effective nucleon coupling taking into account the nucleon content ξ_N [27].

To obtain the frequency-domain signature of Eq. (8), we describe the three frequency components of the amplitude-modulated signal as a carrier at the ALP Compton frequency ω_a and two sidebands A_{\pm} separated from the carrier A by the Earth's sidereal frequency at $\omega_{\pm} = \omega_a \pm \omega_e$. The amplitudes of the three components (in magnetic field units) are given by

$$\begin{aligned} |A| &= g_{\text{eff}}\alpha_z \cos \theta, \\ |A_-| &= g_{\text{eff}} \frac{\sin \theta}{2} \sqrt{\alpha_x^2 + \alpha_y^2 - 2\alpha_x\alpha_y \sin(\phi_x - \phi_y)}, \\ |A_+| &= g_{\text{eff}} \frac{\sin \theta}{2} \sqrt{\alpha_x^2 + \alpha_y^2 + 2\alpha_x\alpha_y \sin(\phi_x - \phi_y)}. \end{aligned} \quad (9)$$

As can be seen from the relationships of A and A_{\pm} to the independent random ALP DM parameters α_i and ϕ_i expressed in Eq. (9), it is evident that the carrier and sideband amplitudes are essentially independent of one another. This means, for example, that the sideband amplitudes are generally asymmetric.

Note that the total power of the gradient of the ALP DM signal within a single coherence patch distributed among three frequencies ω_a , ω_+ , and ω_- is

$$\frac{|A|^2}{\cos^2 \theta} + \frac{2(|A_+|^2 + |A_-|^2)}{\sin^2 \theta} = g_{\text{eff}}^2(\alpha_z^2 + \alpha_x^2 + \alpha_y^2) = g_{\text{eff}}^2|\alpha|^2. \quad (10)$$

In our actual experimental search for ALP DM, it is essential to also consider the role of noise in the comagnetometer data. Correlated measurements of ALP DM with two sensors instead of a single sensor lead to a substantial improvement of sensitivity. In fact, the improvement is greater than a factor of $\sqrt{2}$ [28] which would result from two measurements of a quantity with uncorrelated noise. The reason lies in the respective orientation of the sensitive axes of the two sensors. In our configuration, the combination of both sensors allows access to all spatial components of the ALP gradient signal. The individual ALP gradient components are independent random values described by Rayleigh distributions. Probing all of them simultaneously using the ALP DM interferometer configuration enables us to increase the combined signal amplitude and extend the range of the search into lower values of g_{eff} .

The spatial configuration of the two-station ALP DM interferometer is as follows: the sensitive axis of the Mainz station is horizontal in the laboratory pointing East in the Earth rotation plane ($\theta_M = 90^\circ$), and therefore, is exclusively sensitive to the sideband signal $A(\omega_a \pm \omega_e)$. In contrast, the sensitive axis of the Kraków station is horizontal in the laboratory pointing North ($\theta_K = 50^\circ$). The Kraków station is therefore sensitive to all ALP signatures in the frequency spectrum: carrier and sidebands.

III. SEARCH STRATEGY AND RESULTS

We searched for ALP DM with Compton frequencies up to 11.6 Hz. In this frequency range, the linewidth of the ALP signal is below the frequency resolution of our experiment. Additionally, the sensitive axes of the comagnetometers are modulated at the Earth sidereal frequency, $\omega_e/2\pi \approx 11.6 \mu\text{Hz}$, resulting in sidebands at $\omega_a \pm \omega_e$, see Eq. (9). The expected ratio between the central peak and the sidebands is given by the components of the sensitive axes parallel (carrier) and perpendicular (sidebands) to the rotation axis of the Earth.

The data analyzed in this work correspond to a total of 40 measurement days in Mainz and 28 days in Kraków, collected in a time window of 92 days between Jan. 6th and Apr. 7th, 2024. Continuous data was acquired as much as possible, but several technical interruptions occurred during the measurement campaign. Continuous 25-hour data segments were used for the analysis, ensuring sidereal frequency resolution ($\Delta\omega \lesssim \omega_e$). At the beginning of each segment, both comagnetometers were calibrated. To infer the frequency response of the comagnetometers to exotic interactions, we followed the method reported in Ref. [17]. It consists of (1) measuring the response to a magnetic step perturbation, (2) fitting the data with a model describing the coupled spin dynamics, and (3) inferring the exotic frequency-response from the fit parameters. A summary of the calibration-fit results for Mainz and Kraków is shown in Fig. 6. In this way, each 25-hour block of data had its own measured frequency response function used for calibration after applying the Discrete Fourier Transform (DFT) to the time series data. In general, when searching for unknown dynamic observables, it is of utmost importance to precisely know the frequency response of the sensor. However, for ALP DM, the frequency response cannot be directly measured prior to detection.

A frequency-dependent phase-shift is applied to each DFT subset to ensure that the phase of an ALP DM signal in any frequency bin would be the same throughout all DFT subsets. Then, all DFT subsets of the respective station are averaged, resulting in a mean value and its standard deviation. We confirmed that the time-shifted DFT averaging procedure had no effect on the Fourier coefficients of injected oscillations.

Now we construct an estimator $S(\omega)$ for the ALP DM signal amplitude that can be used to search for ALP signals considering Eq. (10). To get the optimum signal-to-noise ratio we extract all potential ALP signatures from the data by combining the two DFT datasets of Mainz and Kraków and then combining the power of carrier and sidebands.

First, the complex Fourier components of the sidebands (A_{\pm}) in Mainz and Kraków are added with weights taking into account the direction of the sensitive axes and the noise level (see Sec. VB). The interfered sideband sig-

nal then reads

$$A_{\pm}^{K+M} = \frac{a_{\pm}^M A_{\pm}^M + a_{\pm}^K A_{\pm}^K e^{-i(\phi+\pi/2)}}{a_{\pm}^K + a_{\pm}^M}, \quad (11)$$

where a_{\pm}^i are the weights with \pm designating the higher (+) and lower (-) frequency sideband and index $i = M, K$ the Mainz and Kraków stations, respectively. The angle between the positions of the Mainz and Kraków comagnetometers in the rotation plane of the Earth is ϕ , see Fig. 1(b). Accounting for the angle ϕ is required to ensure constructive interference of an oscillating ALP DM signal recorded in the two comagne-

tometers. The constructive interference of the ALP DM signal in the combination of the sidebands is illustrated in Fig. 1(c).

In the second step, we combine the carrier in Kraków A^K with the interfered sideband signal A_{\pm}^{K+M} . The signal estimator $S(\omega)$ is designed to optimize the signal-to-noise ratio for ALP DM through the choice of appropriate weights, a^K for the carrier in Kraków and a_{\pm}^{K+M} for the upper and lower interfered sideband, see Sec. V B. The Mainz carrier signal does not contribute to the signal estimator $S(\omega)$, as its weight $a^M \approx 0$, because $\cos(\theta_M) \approx 0$, meaning that there is no contribution to A^M from ALP DM. The estimator for the ALP DM signal $S(\omega)$ is defined in the following way:

$$S(\omega) = \sqrt{\frac{(a^K)^2 |A^K|^2 + (a_-^{K+M})^2 |A_-^{K+M}|^2 + (a_+^{K+M})^2 |A_+^{K+M}|^2}{(a^K)^2 + (a_-^{K+M})^2 + (a_+^{K+M})^2}}. \quad (12)$$

Note that the standard deviation of the DFTs is propagated accordingly, resulting in an uncertainty in the signal estimator $\Delta S(\omega)$ for each frequency.

The value of $S(\omega)$ in magnetic field units as determined from the acquired data is shown by the blue points in Fig. 2. Given that an ALP DM signal in the $S(\omega)$ data would appear at a single frequency ω_a , we assume that the total of sampled frequencies $S(\omega)$ characterizes the technical noise of our interferometer. To determine whether any of the estimator data points are significantly larger than expected from the measured technical noise a detection threshold is established. The set of signal estimator $S(\omega)$ values normalized with the respective standard deviation at each frequency is empirically found to match a χ distribution with three degrees of freedom. The χ distribution is displaced by the expected noise to take into account nearby bins when claiming a detection. The detection threshold is chosen such that a candidate signal above threshold would have only a 5% global chance of arising due to technical noise which accounts for the look-elsewhere effect.

We determine the expected value of the technical noise amplitude at each frequency based on the measured values at surrounding points. For frequencies below 0.1 Hz the mean is inferred from a global fit assuming a $1/f$ noise model. Above 0.1 Hz the mean is based on the moving average of 500 consecutive points centered around (but excluding) the frequency of interest. Figure 2 shows the mean of the technical noise as an orange line determined as discussed above, as well as a light red line indicating the 95% global significance threshold for each frequency.

For ALP DM with frequencies below ω_e , a different search approach is used. An ALP DM contribution at ω_e would be observed for the Compton frequencies $\omega_a < \omega_e$ even if ω_a cannot be directly resolved in our data. The width of each frequency bin is $\approx \omega_e$. In this situation,

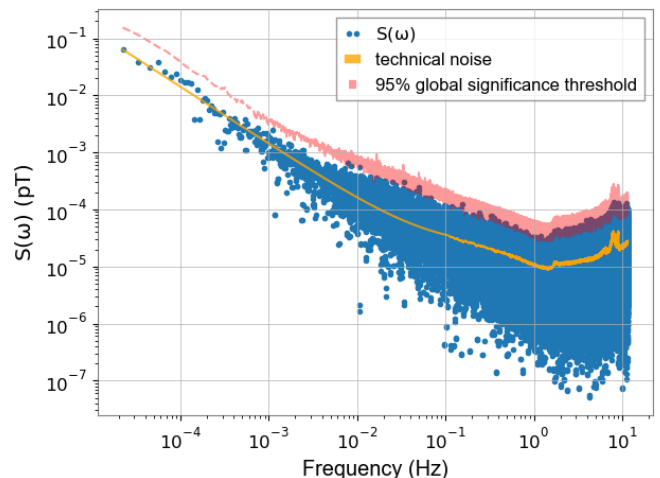


FIG. 2. Signal estimator $S(\omega)$ obtained by interfering Mainz and Kraków comagnetometer data, for frequencies above ω_e . Results are shown as a function of frequency. The data shows a $1/f$ up to 10^{-1} Hz behaviour consistent with technical noise of the apparatus. No ALP candidate is found above the global 95% significance threshold. The peak sensitivity of the estimator reaches 10^{-17} T.

the sidebands are at $\omega_e \pm \omega_a$. Since $\omega_e > \omega_a$ they appear in the same frequency bin at ω_e . By examining the frequency bin at ω_e , the ALP search can be extended to the limit $\omega_a \ll \omega_e$. Due to the particular characteristics of this bin, we do not include it in the general ALP DM search described in the previous paragraph. Instead, we add Mainz and Kraków amplitudes $A^K(\omega) + A^M(\omega)$ with their respective weights for the frequency bin at ω_e as well as for the bins below 0.1 Hz that follow $1/f$ noise model. The resulting values around ω_e give the expected

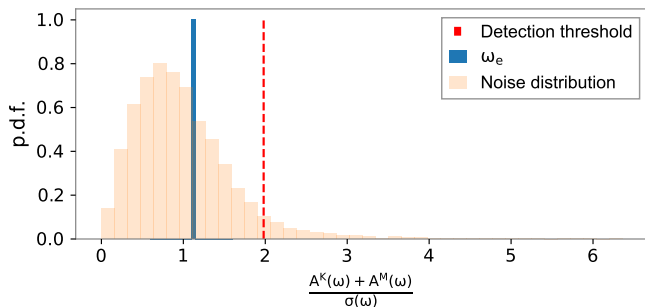


FIG. 3. Histogram of the expected noise distribution and the combined amplitude value at ω_e in function of the measured Fourier amplitude. For an ALP field oscillating below ω_e , the sidebands are not resolved and an ALP signature is present at ω_e . However, $A^{M+K}(\omega_e)$ is compatible with the expected noise distribution and thus no ALP candidates with frequencies $\omega_a < \omega_e$ is reported.

noise distribution matching a Rayleigh distribution, and the searched ALP DM signal would be at ω_e . Results are shown in Fig. 3. The measured amplitude at ω_e is consistent with noise and therefore shows no evidence of an ALP DM candidate.

We do not find any ALP DM candidates in the frequency range from 10^{-8} Hz to 11.6 Hz. We proceed to set limits.

IV. SETTING LIMITS

Since there are no ALP candidates, we set exclusions on the ALP-proton coupling g_{aPP} and ALP-neutron coupling g_{aNN} . For simplicity, we assume $g_{aPP}(g_{aNN}) = 0$ when constraining $g_{aNN}(g_{aPP})$. We describe the exclusion strategy for a generic g_{eff} coupling to the nucleus that is rescaled by the respective nucleon contributions ξ_P and ξ_N to the total nuclear spin to get the final exclusions for proton and neutron coupling $g_{aPP} = g_{\text{eff}}/\xi_P$ and $g_{aNN} = g_{\text{eff}}/\xi_N$.

To compute upper limits on the ALP-coupling strength we take into account both the measured noise properties of $S(\omega)$ and the distribution of ALP DM signals $S_{g_{\text{eff}}}(\omega)$ for a given ALP-coupling strength g_{eff} based on our assumed model of ALP DM. The ALP DM signal $S_{g_{\text{eff}}}(\omega)$ is calculated from Eq. (12) based on the ALP DM field parameters characterized by the probability distribution from Eq. (9), accounting for the stochastic properties of ALP DM (Section II).

We use the Confidence Levels (CLs) method [29] to determine the limits on the coupling strength g_{eff} . If the measured value $S(\omega)$ is purely due to noise, it can be represented by a random number X_n drawn from a χ distribution with a scale parameter determined by the uncertainty $\Delta S(\omega)$. The potential contribution to $S(\omega)$ from an ALP DM signal can also be represented by a random number accounting for its stochastic nature. We

compute this with Monte Carlo simulations and scaled the ALP DM distribution with the interaction strength g_{eff} . Finally, we add the noise distribution to the signal distribution and draw from the combined distribution a random number X_{S+n} .

A certain value of g_{eff} is excluded with a confidence limit $CL = 95\%$ at frequency ω when

$$\frac{\mathbb{P}(X_{S+n} \leq S(\omega))}{\mathbb{P}(X_n \leq S(\omega))} \leq 1 - CL = 0.05, \quad (13)$$

where \mathbb{P} indicates the probability. The condition described by Eq. (13) means that for the excluded value of g_{eff} , there is only a 5% relative probability that an ALP DM signal contributes to the measured value of $S(\omega)$.

The sidereal frequency bin at ω_e is used to expand the search to frequencies below 10^{-5} Hz. Due to constraints on ALP masses below $m_a = 10^{-22}$ eV/ c^2 [9], the exclusion from the sidereal frequency bin is limited from 2.4×10^{-8} Hz to the sidereal frequency $\omega_e/2\pi \approx 1.1 \times 10^{-5}$ Hz. In this range, the field is considered nearly constant ($\omega_a \approx 0$). For a single station, the expected signal defined in Eq. (8) becomes

$$\lim_{\omega_a \rightarrow 0} \nabla a(t) \cdot \hat{\mathbf{m}}(t) = \sin \theta \left\{ \alpha_x \cos \phi_x \sin(\omega_e t + \phi_e) + \alpha_y \cos \phi_y \cos(\omega_e t + \phi_e) \right\}. \quad (14)$$

Therefore, the oscillating signal expected in the sensor is driven only by the rotation of the Earth at ω_e with an amplitude

$$A_{\omega_e} = g_{\text{eff}} \sin \theta \sqrt{(\alpha_x \cos \phi_x)^2 + (\alpha_y \cos \phi_y)^2}, \quad (15)$$

In contrast to the case of $\omega_a > \omega_e$ (shown in Eq. (10)), the ALP DM signal amplitude explicitly depends on the random phases ϕ_x and ϕ_y . In this regime, where $\omega_a \approx 0$, the stations sample less than a period of the ALP DM field; and there is a probability of measuring near a zero crossing (when $A_{\omega_e} \approx 0$). To account for this situation and the intermediate regime, where some of the ALP DM oscillation is still measured, we perform Monte Carlo simulations of the integrated power of the respective oscillation fractions

$$\propto \frac{1}{T} \int_0^T dt [\alpha_x^2 \cos^2(\omega_a t + \phi_x) + \alpha_y^2 \cos^2(\omega_a t + \phi_y)] \quad (16)$$

for uniformly distributed phases ϕ_x and ϕ_y and the respective ω_a .

For frequencies around 10^{-1} Hz, the total measurement time is on the order of the coherence time. The ALP oscillation is coherent for measurement times $T \lesssim \tau_{\omega_a}/2.5$ [23, 28]. In particular, for frequencies $\omega_a/2\pi \gtrsim 5 \times 10^{-2}$ Hz the ALP field is not coherent over the entire measurement time (92 d). Therefore, for frequencies above 5×10^{-2} Hz, we multiply our estimated

constraints on the coupling constants by $\sqrt{T/\tau\omega_a}$ to account for the incoherent averaging.

The final results of this work are constraints in both proton and neutron ALP coupling g_{aNN} and g_{aPP} . The excluded parameter space covers a frequency range from 10^{-8} Hz to 11.6 Hz, corresponding to masses from 10^{-22} eV to 4×10^{-14} eV, a total of nine orders of magnitude. Figure 4 shows the constrained parameter space in the context of previous laboratory searches. In the mass range of $1.2 - 4 \times 10^{-17}$ eV the exclusion improves previous constraints by 3-4 orders of magnitude.

Note that we do not include the results of Ref. [30] in Figs. 4 or 5. Reference [30] presented a re-analysis of comagnetometer data from the Princeton group acquired in three different experiments [31–33]. More recently, the Princeton group published their own re-analysis of their data in Ref. [18], which notes critical issues in the interpretation of their data not accounted for in Ref. [30]. We regard the more recent Ref. [18] as the definitive interpretation of the data from the Princeton comagnetometer experiments.

Both comagnetometers in Mainz and Kraków are part of the Advanced Global Network of Magnetometers for Exotic physics searches (GNOME) experiment [34]. Other comagnetometers are in development and will join future science runs allowing for an increased sensitivity to ALP DM as well as to transient events. Transient event searches greatly benefit from a network of more than two sensors.

At the same time, this experiment is part of the CASPER family of experiments [35, 36], significantly improving on the previous CASPER results in this frequency range, see Figs. 4 and 5.

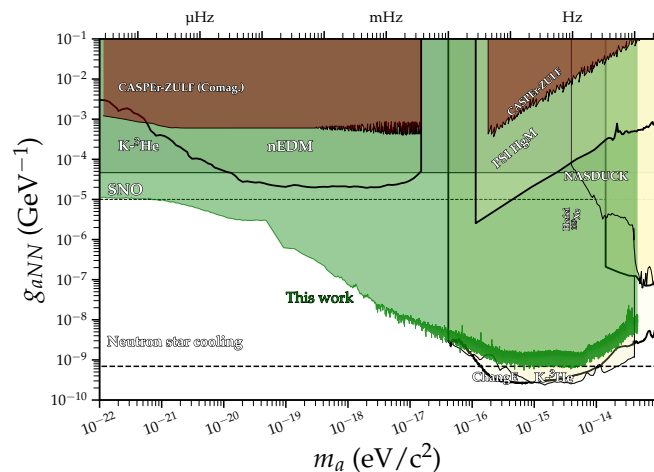


FIG. 4. Exclusion plot for neutron coupling. Other laboratory (solid lines) and astrophysical (dashed lines) constraints are shown for reference and extracted from [37]: CASPER-ZULF [35, 36], $K-^3\text{He}$ [18, 33], nEDM [38], PSI HgM [39], SNO [40], NASDUCK [41], Hefei ^{129}Xe [42], ChangE [19], and neutron star cooling [43].

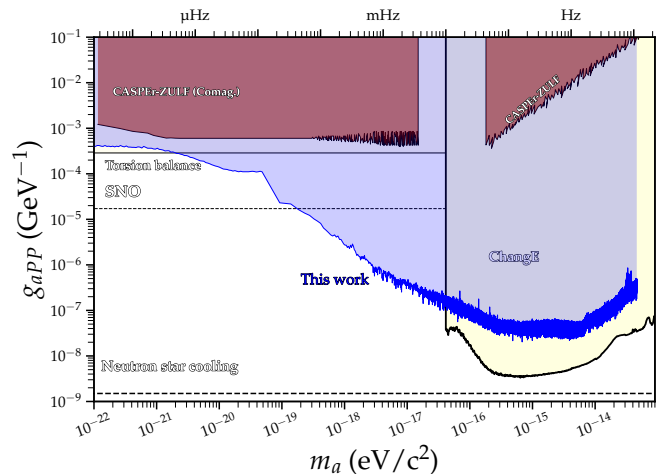


FIG. 5. Exclusion plot for proton coupling. Other laboratory (solid lines) and astrophysical (dashed lines) constraints are shown for reference and extracted from [37]: CASPER-ZULF [35, 36], ChangE [19], and neutron star cooling [43].

V. METHODS

A. Experimental set up

The interferometer is composed of two self-compensating comagnetometers located about 1000 km apart: one in Mainz, Germany, the second one in Kraków, Poland. The two self-compensated comagnetometer systems are similar to that reported in Refs. [15, 17]. At the core of each comagnetometer system is a spherical cell heated to about 180°C and mounted inside a four-layer magnetic shield. The cell is filled with 3 μm of ^3He and 50 Torr of N_2 and loaded with a drop of an alkali-metal mixture with 1% ^{87}Rb and 99% natural-abundance K (molar fractions). Spins are optically pumped with a $\sim 30 \text{ mW}/\text{cm}^2$ circularly-polarized light tuned to the center of the Rb D_1 line. The readout is realized by monitoring the polarization rotation of a $\sim 15 \text{ mW}/\text{cm}^2$ linearly-polarized light detuned about 0.5 nm from the K D_1 line. To reduce the influence of the magnetic field noise at low frequencies, the comagnetometers are operated in the self-compensating regime [13]. To operate in this regime, a B_z (compensation) field of about 100 nT is applied. In the Mainz comagnetometer we modulate the B_x field with a 80 Hz sine wave. The signal detuned at that frequency exhibits a resonance that is used to lock the system to the compensation point and avoid the slow drift of equilibrium compensation field [15]. Following the calibration procedure described in Ref. [17], the sensitivity of both comagnetometers to exotic nucleon couplings is estimated with a daily (every 25 h) calibration pulse. In the Kraków comagnetometer the drifts from the compensation point are corrected after each calibration pulse. The response to the calibration pulse

is fitted with the system parameters. The parameters of the fit include the amplitude of the response that relates the voltage output to pseudo-magnetic fields, the detuning from the compensation point ΔB_z , the Larmor frequency of both electron ω_e and ${}^3\text{He}$ nucleus ω_n and the relaxation rate of electrons R_e . In the current stage of the work, nuclear relaxation R_n is ignored. Figure 6 summarizes the fit parameters. There is little variance in the parameters during the whole run. The detuning from the compensation point ΔB_z remains below 2 nT, which is within 2% of to the leading field (~ 100 nT).

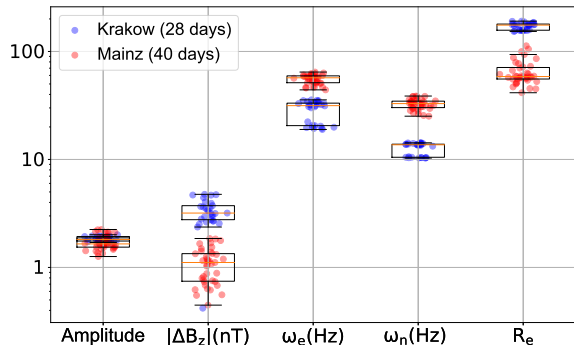


FIG. 6. Summary of the frequency response fit results used for sensor calibration in Mainz and Kraków. The fit parameters are described in detail in Ref. [17].

B. Weights of the ALP signal estimator $S(\omega)$

The weights used in the signal estimator [see Eq. (11) and Eq. (12)] are defined in the following way

$$\begin{aligned}
 a^M &= \frac{2 \cos \theta_M}{(\sigma^M)^2} \approx 0, \\
 a^K &= \frac{2 \cos \theta_K}{(\sigma^K)^2}, \\
 a_{\pm}^M &= \frac{\sin \theta_M}{(\sigma_{\pm}^M)^2}, \\
 a_{\pm}^K &= \frac{\sin \theta_K}{(\sigma_{\pm}^K)^2},
 \end{aligned} \tag{17}$$

where a_{\pm}^i are the weights with \pm designating the higher (+) and lower (-) frequency sideband and index $i = M, K$ the Mainz and Kraków stations, respectively. The σ represents the standard deviation of the Mainz and Kraków amplitudes in the frequency bin of interest. For the interfered sidebands, the weights are resulting from error propagation of a_{\pm}^{K+M} according to Eq. (11). The factor 2 in a^M and a^K is given by the expected ALP DM signal in the carrier being twice the sidebands, see Eq. (9).

VI. ACKNOWLEDGMENTS

We would like to acknowledge Gary Centers, Wolfgang Gradl, Julian Walter and Yuzhe Zang for helpful discussion. We acknowledge support by the German Research Foundation (DFG) within the German Excellence Strategy (Project ID 39083149); by work from COST Action COSMIC WISPerS CA21106, supported by COST (European Cooperation in Science and Technology). SP acknowledge support from the National Science Center, Poland within the OPUS program (2020/39/B/ST2/01524) and GL acknowledges support from the Excellence Initiative – Research University of Jagiellonian University in Krakow. The work of DFJK was supported by the U.S. National Science Foundation under grant PHYS-2110388. The work of AOS was supported by the U.S. National Science Foundation CAREER grant PHY-2145162, and by the Gordon and Betty Moore Foundation, grant DOI 10.37807/gbmf12248.

-
- [1] G. Bertone, D. Hooper, and J. Silk, Particle dark matter: evidence, candidates and constraints, *Phys. Rep.* **405**, 279 (2005).
- [2] J. L. Feng, Dark Matter Candidates from Particle Physics and Methods of Detection, *Annual Review of Astronomy and Astrophysics*, 495 (2010).
- [3] P. Gorenstein and W. Tucker, Astronomical Signatures of Dark Matter, *Adv. High Energy Phys.* **2014**, 10.1155/2014/878203 (2014).
- [4] D. Antypas, A. Banerjee, C. Bartram, M. Baryakhtar, J. Betz, *et al.*, New Horizons: Scalar and Vector Ultralight Dark Matter, arXiv 10.48550/arXiv.2203.14915 (2022), 2203.14915.
- [5] R. T. Co, L. J. Hall, and K. Harigaya, Axion Kinetic Misalignment Mechanism, *Physical Review Letters* **124**, 251802 (2020).
- [6] D. J. E. Marsh, Axion cosmology, *Phys. Rep.* **643**, 1 (2016).
- [7] P. W. Graham and S. Rajendran, New observables for direct detection of axion dark matter, *Phys. Rev. D* **88**, 035023 (2013).
- [8] D. Budker, P. W. Graham, M. Ledbetter, S. Rajendran, and A. O. Sushkov, Proposal for a Cosmic Axion Spin Precession Experiment (CASPEr), *Physical Review X* **4**, 021030 (2014).
- [9] D. F. Jackson Kimball and K. Van Bibber, eds., *The Search for Ultralight Bosonic Dark Matter* (Springer International Publishing, Cham, 2023).
- [10] P. W. Graham, I. G. Irastorza, S. K. Lamoreaux, A. Lindner, and K. A. v. Bibber, Experimental Searches for the Axion and Axion-Like Particles, *Annual Review of Nuclear and Particle Science* **65**, 485 (2015), publisher: Annual Reviews.
- [11] N. Crescini, *The Fermionic Axion Interferometer* (2023).
- [12] T. E. H. T. Collaboration, Akiyama, *et al.*, First M87 Event Horizon Telescope Results. I. The Shadow of the Supermassive Black Hole, *The Astrophysical Journal Letters* **875**, L1 (2019).
- [13] T. W. Kornack and M. V. Romalis, Dynamics of Two Overlapping Spin Ensembles Interacting by Spin Exchange, *Physical Review Letters* **89**, 253002 (2002).
- [14] K. Wei, T. Zhao, X. Fang, Z. Xu, C. Liu, *et al.*, Ultrasensitive Atomic Comagnetometer with Enhanced Nuclear Spin Coherence, *Physical Review Letters* **130**, 063201 (2023).
- [15] E. Klinger, T. Liu, M. Padniuk, M. Engler, T. Kornack, *et al.*, Optimization of nuclear polarization in an alkali-noble gas comagnetometer, *Phys. Rev. Appl.* **19**, 044092 (2023).
- [16] M. Padniuk, M. Kopciuch, R. Cipolletti, A. Wickenbrock, D. Budker, and S. Pustelny, Response of atomic spin-based sensors to magnetic and nonmagnetic perturbations, *Scientific Reports* **12**, 324 (2022).
- [17] M. Padniuk, E. Klinger, G. Łukasiewicz, D. Gavilan-Martin, T. Liu, *et al.*, Universal determination of comagnetometer response to spin couplings, *Physical Review Research* **6**, 013339 (2024).
- [18] J. Lee, M. Lisanti, W. A. Terrano, and M. Romalis, Laboratory Constraints on the Neutron-Spin Coupling of feV-Scale Axions, *Physical Review X* **13**, 011050 (2023), publisher: American Physical Society.
- [19] K. Wei, Z. Xu, Y. He, X. Ma, X. Heng, *et al.*, *Dark matter search with a strongly-coupled hybrid spin system* (2023).
- [20] Z. Xu, X. Ma, K. Wei, Y. He, X. Heng, *et al.*, Constraining ultralight dark matter through an accelerated resonant search, *Communications Physics* **7**, 1 (2024).
- [21] F. Chadha-Day, J. Ellis, and D. J. E. Marsh, Axion dark matter: What is it and why now?, *Science Advances* **8**, eabj3618 (2022).
- [22] J. W. Foster, N. L. Rodd, and B. R. Safdi, Revealing the dark matter halo with axion direct detection, *Physical Review D* **97**, 123006 (2018).
- [23] G. P. Centers, J. W. Blanchard, J. Conrad, N. L. Figueroa, A. Garcon, *et al.*, Stochastic fluctuations of bosonic dark matter, *Nature Communications* **12**, 7321 (2021).
- [24] M. Lisanti, M. Moschella, and W. Terrano, Stochastic properties of ultralight scalar field gradients, *Physical Review D* **104**, 055037 (2021).
- [25] A. V. Gramolin, A. Wickenbrock, D. Aybas, H. Bekker, D. Budker, *et al.*, Spectral signatures of axionlike dark matter, *Physical Review D* **105**, 035029 (2022).
- [26] V. Flambaum and I. Samsonov, Fluctuations of atomic energy levels due to axion dark matter, *Physical Review D* **108**, 075022 (2023).
- [27] D. F. J. Kimball, Nuclear spin content and constraints on exotic spin-dependent couplings, *New Journal of Physics* **17**, 073008 (2015), publisher: IOP Publishing.
- [28] A. Derevianko, Detecting dark-matter waves with a network of precision-measurement tools, *Physical Review A* **97**, 042506 (2018).
- [29] A. L. Read, Presentation of search results: the CLs technique, *Journal of Physics G: Nuclear and Particle Physics* **28**, 2693 (2002).
- [30] I. M. Bloch, Y. Hochberg, E. Kuflik, and T. Volansky, Axion-like relics: new constraints from old comagnetometer data, *Journal of High Energy Physics* **2020**, 167 (2020).
- [31] G. Vasilakis, J. M. Brown, T. W. Kornack, and M. V. Romalis, Limits on New Long Range Nuclear Spin-Dependent Forces Set with a K – He 3 Comagnetometer, *Physical Review Letters* **103**, 261801 (2009).
- [32] J. M. Brown, S. J. Smullin, T. W. Kornack, and M. V. Romalis, New Limit on Lorentz- and CPT-Violating Neutron Spin Interactions, *Physical Review Letters* **105**, 10.1103/PhysRevLett.105.151604 (2010).
- [33] J. Lee, A. Almasi, and M. Romalis, Improved Limits on Spin-Mass Interactions, *Physical Review Letters* **120**, 161801 (2018).
- [34] S. Afach, D. Aybas Tumturk, H. Bekker, B. C. Buchler, D. Budker, *et al.*, What Can a GNOME Do? Search Targets for the Global Network of Optical Magnetometers for Exotic Physics Searches, *Annalen der Physik* **536**, 2300083 (2023).
- [35] A. Garcon, J. W. Blanchard, G. P. Centers, N. L. Figueroa, P. W. Graham, *et al.*, Constraints on bosonic dark matter from ultralow-field nuclear magnetic resonance, *Science Advances* **5**, eaax4539 (2019).
- [36] T. Wu, J. W. Blanchard, G. P. Centers, N. L. Figueroa, A. Garcon, *et al.*, Search for Axionlike Dark Matter with a Liquid-State Nuclear Spin Comagnetometer, *Physical Review Letters* **122**, 191302 (2019).

- [37] C. O'Hare, [cajohare/axionlimits: Axionlimits](https://cajohare.github.io/AxionLimits/), <https://cajohare.github.io/AxionLimits/> (2020).
- [38] C. Abel, N. Ayres, G. Ban, G. Bison, K. Bodek, *et al.*, Search for Axionlike Dark Matter through Nuclear Spin Precession in Electric and Magnetic Fields, *Physical Review X* **7**, 041034 (2017).
- [39] C. Abel, N. J. Ayres, G. Ban, G. Bison, K. Bodek, *et al.*, Search for ultralight axion dark matter in a side-band analysis of a ^{199}Hg free-spin precession signal, *SciPost Physics* **15**, 058 (2023).
- [40] A. Bhusal, N. Houston, and T. Li, Searching for Solar Axions Using Data from the Sudbury Neutrino Observatory, *Physical Review Letters* **126**, 091601 (2021).
- [41] I. M. Bloch, R. Shaham, Y. Hochberg, E. Kuflik, T. Volansky, and O. Katz, *NASDUCK SERF: New constraints on axion-like dark matter from a SERF comagnetometer* (2022).
- [42] M. Jiang, H. Su, A. Garcon, X. Peng, and D. Budker, Search for axion-like dark matter with spin-based amplifiers, *Nature Physics* **17**, 1402 (2021).
- [43] M. Buschmann, C. Dessert, J. W. Foster, A. J. Long, and B. R. Safdi, Upper Limit on the QCD Axion Mass from Isolated Neutron Star Cooling, *Physical Review Letters* **128**, 091102 (2022).